Detailed Kinetic Monte Carlo Simulations of Graphene-Edge Growth

Russell Whitesides and Michael Frenklach*

Department of Mechanical Engineering, University of California, and Environmental Energy Technologies Division, Lawrence Berkeley National Laboratory, Berkeley, California 94720

Received: July 10, 2009; Revised Manuscript Received: November 18, 2009

A new detailed chemical-kinetic Monte Carlo model of graphene-edge growth is presented. The model employs a fine-grained approach to chemically resolved species, allows for incorporation of five-member rings into growing structures, and links the stochastic kinetic steps to a geometry optimization, thereby properly accounting for curving of molecular structures. The evolving morphology is greatly affected by the rates of key reactions and hence by surface-site steric environment and gas-phase species concentrations. The evolving graphene morphology and growth rates seemingly reach "asymptotic" behavior, independent of the initial substrate. Most noteworthy, growing layers become significantly curved. The curvature occurs regardless of initial substrate at both 1500 and 2000 K with higher curvature occurring at the lower temperature. More intriguing is the observation that, at 2000 K, transition from planar to curved growth does not commence immediately but occurs at some later time, seemingly when the growing graphene reaches a size significantly larger than coronene. No curvature is produced in numerical simulations at 2500 K, indicating that high-energy environments cause the five-member-ring to be less stable, thus preventing them from forming.

I. Introduction

Graphene. Graphene, a single sheet of graphite, has recently gained substantial interest in the areas of condensed-matter physics and materials science due its unique properties such as high electrical conductivity,[1−3] superior thermal conductivity,[4] and intrinsic strength.[5] The envisioned applications of free-standing graphene sheets are broad[6] and include composites,[7] electronic devices,[8] sensors,[9] photodetectors,[10] batteries,[11,12] ultracapacitors,[13] and imaging substrates.[14] The current methods of producing graphene sheets are mechanical exfoliation of graphite[15,16] (i.e., peeling off layers with scotch tape), chemical reduction of exfoliated graphite oxide,[17−19] vacuum graphitization of silicon carbide substrates,[20] chemical vapor deposition on substrates,[21−29] and substrate-free gas-phase synthesis.[30−33]

Graphene substrates have also become an important surrogate for theoretical studies of carbonaceous (soot and interstellar-dust) particle surface[34−39] because such particles are composed of graphitic elements.[40−43] Understanding the chemical mechanisms underlying the growth of soot in high-temperature environments, such as flames, has progressed substantially in recent years. Our objective here is to summarize the current knowledge and present an emerging model of graphene-edge growth, resolved at elementary-reaction level. In addition to approaching the goal of developing predictive models of soot formation in combustion, the gained knowledge may also assist in seeking mass-production methods of graphene synthesis.

Mechanism of Graphene-Edge Growth. It has been established in experimental studies that acetylene is the principal gaseous growth species that reacts at the soot particle surface, and that this carbon deposition process follows first-order kinetics.[44−46] Theoretical treatment of surface reactions was initiated by introduction of the hypothesis of chemical similarity, which postulated that chemical reactions taking place on soot particle surface are analogous to those of large PAHs.[47−49] In other words, the surface of soot particles was assumed to look chemically like an edge of a large PAH molecule, covered with C−H bonds. The gaseous environment forming soot is usually dominated by acetylene for molecular growth species and by hydrogen atoms for radicals, and the growth of carbon mass was suggested to follow the hydrogen-abstraction-C_2H_2-addition (HACA) mechanism,[49,50] a repetitive sequence in which a surface radical site is created by hydrogen abstraction and subsequent acetylene addition to the created surface radical forms an aromatic ring,

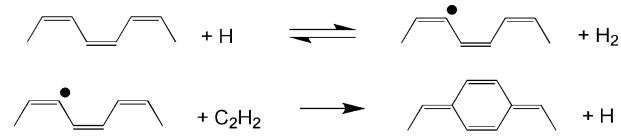

The initial HACA mechanism for surface growth was based on the armchair edge of aromatics,[48,50] as depicted above. However, there is no experimental or theoretical evidence indicating the growing surface has to be exclusively armchair. Furthermore, it was later noted that applying the HACA mechanism to a graphene armchair edge of a finite size leads to the formation and persistence of zigzag edges.[34] It was also noted[34] that application of the HACA mechanism to zigzag edges results in the formation of five-member rings. A follow-up study[51] corroborated that five-member ring adsorption can proceed via a similar mechanism and with a similar rate to those of the "canonical" HACA reaction mechanism. The same study presented a mechanism for five-member ring migration, which included a triradical species as an intermediate.

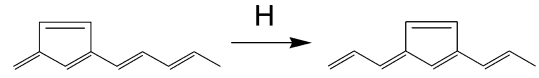

Frenklach, Schuetz and Ping (FSP)[36] found a more plausible five-member ring migration mechanism with only monoradical

* To whom correspondence should be addressed. Phone: 510-643-1676. E-mail: myf@me.berkeley.edu.

10.1021/jp906541a
Published on Web 12/14/2009

Russell Whitesides earned his B.S. and Ph.D. degrees in Mechanical Engineering from Virginia Commonwealth University and the University of California at Berkeley, respectively. His dissertation research focused on the chemistry of aromatic edges. He is now a post-doctoral researcher at Lawrence Livermore National Laboratory performing fluid-dynamic modeling of internal combustion engines.

Michael Frenklach is Professor in the Department of Mechanical Engineering of the University of California at Berkeley. He received his Diploma in Chemical Technology from the Mendeleyev Chemical-Technological University, Moscow, Russia, and his Ph.D. in Physical Chemistry at Hebrew University, Jerusalem, Israel. His faculty appointments began in 1979 in the Department of Chemical Engineering at Louisiana State University. In 1985 he joined the Materials Science Department of the Pennsylvania State University, and in 1995 he accepted his current position at Berkeley. Professor Frenklach's research interests are primarily in the area of chemical-kinetic modeling and elucidation of reaction mechanisms of complex reaction networks, including combustion chemistry, inception and growth of particulate matter, and chemical-vapor deposition of diamond. His current activities focus on global system approach to predictive modeling and uncertainty quantification.

intermediates and lower barriers. The authors performed sterically resolved kinetic Monte Carlo (KMC) simulations by employing the lone-ring migration reaction, shown above, along with adsorption, desorption, and growth steps. The KMC model made use of the steady-state assumption for all radical intermediates to reduce the computational expense of the calculations. The model was able to match initial soot growth rates observed in premixed ethylene−oxygen flame studies of Harris and Weiner.[44] The authors concluded that competition between migration of five-member rings along the zigzag edge and nucleation of six-member rings was a key mechanistic feature dictating growth rate and morphology. An important implication of the migration phenomenon is that while five-member rings are constantly being formed on the growing edge, they do not accumulate; rather, they are converted to six-member rings.

FSP also noted the possibility of five-member rings migrating toward each other and "colliding",

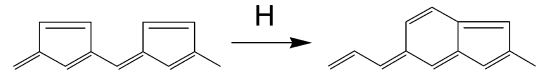

Whitesides et al.[52] investigated the energetics and kinetics of this ring-collision reaction and found that its rate was comparable to the rate of lone-ring migration.[36] They re-examined the lone-ring migration, including additional reaction products, and found that ring desorption is coupled to ring migration and that radical intermediates on both the migration and collision pathways had lifetimes exceeding microseconds at flame conditions. Both of these conclusions indicated a need for a more detailed description of surface species and processes than was used in the FSP simulations.

Further theoretical analysis by Whitesides et al.[53] revealed that the product of the ring collision can undergo isomerization to reverse its orientation, or "flip". The viability of the flip

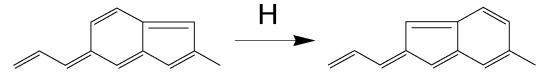

reaction motivated study[54] that identified the phenomenon we call embedded-ring migration, in which a five-member ring moves *through* the zigzag edge of a graphene layer. Theoretical

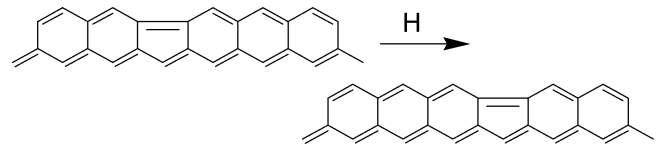

rate coefficients were found to be comparable to the previously investigated flip reaction and other competitive zigzag-edge reactions. The fast kinetics indicated that the embedded ring moves essentially freely within the zigzag edge. On larger substrates, the reaction has a weak thermodynamic preference for configurations with the five-member ring in the interior of the edge as opposed to at the corner, causing embedded rings to be found more often away from the corner of zigzag edges. In spite of this slight thermodynamic tendency, the occurrence of the embedded-ring migration reaction gives embedded rings ample access to the edge corner where they may interact with migrating rings or with gas-phase species. The high mobility of embedded rings enables the layer to minimize the inclusion of five-member rings, and thus should contribute significantly to annealing and smoothing of growing surfaces.

Kraft and co-workers have developed a KMC model[37−39] that follows the form of the FSP model. In their initial formulation[37] the model included the reactions of the FSP model and added edge oxidation. The KMC model was then linked to a soot population balance through statistical information gathered from simulations of single layers and used in simulations of a soot particle formation in a plug-flow reactor[55] and laminar premixed flames.[56] The most recent study[39] included aromatic bay closure reactions[57,58] along with embedded-ring migration[58] and benzene addition to radical edge sites.[59] That study showed agreement between simulation results and experimental measurements for H-to-C ratios of PAH forming in acetylene and benzene flames.

Related studies have been carried out by Violi and co-workers.[60−67] Their work has focused on soot particle inception with small (2−3 ring) aromatic molecules used as growth species, employing the numerical technique[60] that couples KMC with molecular dynamics (MD).[68−73] The reaction steps in the initial model[60,61]

included radical combination reactions of naphthalene and acenaphthylene and aromatic ring closure. Later work[62,63] included C_1 through C_4 species as growth components and found C_2H_2 to be the most prevalent nonaromatic growth species. Violi also investigated the following reaction[58]

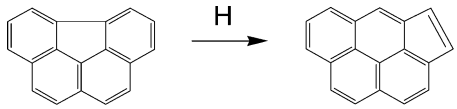

which is the smallest analog of the embedded-ring migration, and considered oxidation reactions.[64] More recent studies have focused on clustering of aromatic molecules formed from the KMC/MD simulations.[65−67] However, surface processes aside from ring closure were not considered.

Here we present a new kinetic Monte Carlo model for graphene-edge growth, built on accumulated knowledge of elementary reaction processes. The model employs a more detailed description of surface reactions and sites and includes many more reactions creating five- and six-member ring complexes. Incorporation of five-member rings leads to graphene sheet curvature and so the KMC model is linked to a molecular mechanics (MM) geometry optimization to account for the resulting structures. Our focus remains on *growth* of graphene and so oxidation is not included.

II. Methodology

The KMC simulations tracked a single graphene "molecule" evolving in a flame environment. At each time step, a reaction event was selected stochastically and then applied. The methodology for specifying these reactions followed Frenklach et al.[36] The simulation was treated as a series of Markov processes, i.e., each subsequent simulation step was only dependent on the current simulation state and not on the previous states. The selection of the reaction event and specific graphene-edge site was done by application of the Gillespie algorithm[74] adapted for surface processes.[75] In short, given a current state at time t_n, the time of the next reaction event at surface site i, $t_{n+1,i}$, was evaluated as

$$t_{n+1,i} = t_n - \frac{\ln u}{k_{\text{total},i}}$$

where u is a random number distributed uniformly between zero and one and $k_{\text{total},i}$ is the sum of the rates of the j reactions possible at site i, $k_{j,i}$,

$$k_{\text{total},i} = \sum_j k_{j,i}$$

The smallest of the $t_{n+1,i}$ determined the time instant, t_{n+1}, and hence the site, i, of the next KMC step. The selection of the particular reaction that occurs at that time was done by comparing the rate-constant ratios computed for site i,

$$p_{j,i} = \frac{k_{j,i}}{k_{\text{total},i}}$$

with another random number u, again distributed uniformly between zero and one. The selected reaction was applied to the selected site, the time was advanced to t_{n+1}, and the process was repeated until the simulation ended.

The first modification of the FSP model[36] was inclusion of more individually resolved surface species. The steady-state assumption used for intermediate elementary reactions of "single step" transformation, applied to speed up the numerical simulation, was found to be inadequate in many cases due to long-lived intermediates.[52,53] Removal of these assumptions necessitated a more "fine-grained" description of surface processes and hence of surface species.

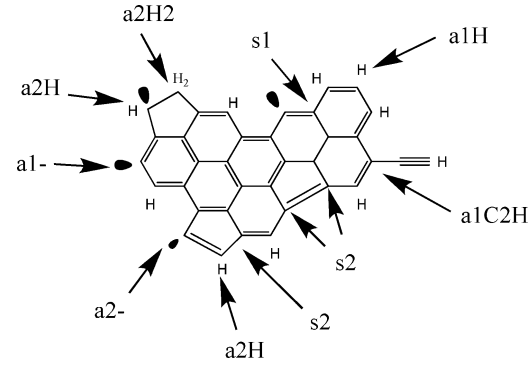

Figure 1. Carbon atom types for kinetic Monte Carlo reaction selection.

In the current model, nine surface species were defined and classified as either active (bonded to two other surface carbon atoms) or solid (bonded to three other surface carbon atoms). There are six active carbon atom species: hydrogen terminated six-member ring carbon atoms (a1H), hydrogen terminated five-member ring carbon atoms (a2H), radical six-member ring carbon atoms (a1-), radical five-member ring carbon atoms (a2-), five-member ring carbon atoms bonded to two hydrogen atoms (a2H2), and six-member ring carbon atoms bonded to a C_2H moiety (a1C2H). There are two classifications for solid carbon species (i.e., bonded to three other carbon atoms), those that are part of six member rings (s1) and those that are part of five and six-member rings (s2). Figure 1 illustrates the six active carbon atoms and two solid carbon atoms. Note that a lower case "a" is used in these designations for carbon atoms to differentiate them from the notation A_1, A_2, ... used to describe free aromatic molecules of varying sizes.[76,77] In addition to the site types shown in Figure 1, one more type was included, "a1solid". It designates a nonreactive site, the type occurring at the bottom edge of a graphene substrate, used in the present study to simulate larger substrates, as shown in Figure 2.

A total of 42 surface transformations were included in the present model and are depicted in Table 1. Reactions forming five- and six-member ring complexes (14, 33, 34, and 39) and those capping embedded five-member rings (35−38) are of particular interest. Rate coefficients for the reactions were taken from experimental data, quantum chemical calculations, or assigned on the basis of analogy to other reactions when data were not available. A detailed account of assignments and sources for the reaction rate coefficients is provided in the Supporting Information.

Initial simulations with the new KMC model revealed that five-member rings are incorporated into the growing substrate layer and cause the structure to curve. This indicated that the developing molecular geometry cannot be described by a two-dimensional lattice as it was previously.[36,39] To properly account for the evolving curvature, the KMC model was coupled to molecular-mechanics geometry optimization using the MM3 potential[78] with the TINKER molecular mechanics package.[79] The MM3 potential has been found to produce geometries for fullerenes in good agreement with the ab initio Hartree−Fock method[80] as well as experimental and DFT results for fullerenic fragments.[81] Optimization of structure geometry was performed after each structure-changing event. The geometry optimization

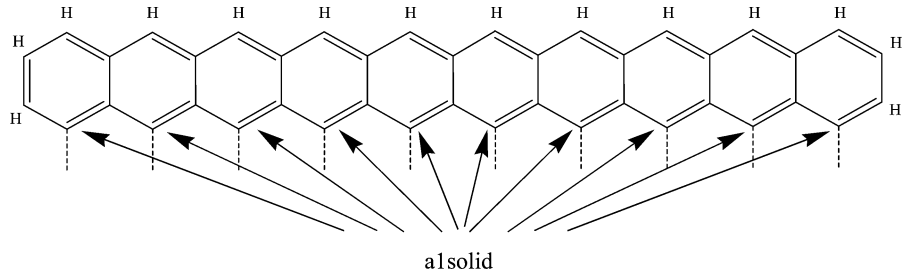

Figure 2. Example substrate of decacene showing a1solid type atoms.

step properly accounted for substrate curvature while maintaining physically accurate bonding and geometric configuration of the growing structures. A check was made after each geometry optimization to ensure that the geometry produced by the molecular mechanics code was consistent with the bonding implied by the KMC model. Specifically, we tested if the geometry optimization left all the carbon atoms within a specified distance of the other atoms to which they were bonded in the KMC description. If any two bonded carbons were found to be separated by more than two angstroms, the simulation was ended. Further details can be found elsewhere.[82]

The computations were performed with an in-house code written in Matlab and executed on a computer cluster equipped with 2 GHz Intel Xeon processors. Computational times of individual runs varied depending on simulated conditions, ranging from about 10 min to a few hours on a single processor for simulated time of 5 ms.

III. Results and Discussion

The KMC simulations were run for a series of conditions. The simulations were performed at temperatures of 1500, 2000, and 2500 K. These temperatures were chosen to bracket the range of soot appearance in combustion. The base gas-phase composition was set to $x_{C_2H_2} = x_{H_2} = 0.1$, $x_H = 0.01$, and $x_{CH_3} = 0$. This set of species mole fractions is equal to those from previous simulations[34,36] and is motivated by laminar flame studies.[48,83]

Bearing in mind the exploratory nature of the present study, each KMC simulation was performed at a constant temperature and gas-phase composition. This allowed us to investigate "in isolation" the effects of key experimental parameters, temperature, and major growth species concentrations. The phenomena exposed by the present study facilitate interpretation of realistic environments, which are typically convoluted by nonlinear interactions present in the growing environment, large uncertainties in the mechanisms and rates of aromatics formation and growth, and still missing knowledge of some critical parts of the overall process, such as particle nucleation.

In the first series of simulations, graphene morphologies resulting from growth of pyrene were examined. Next, the effect of initial substrate geometry was studied. Then, the effect of excluding certain sets of reactions from the kinetic mechanism was analyzed. Finally, the effect of changing the gas-phase composition was investigated.

Zipper Growth. To help in understanding the results, we begin by discussing a key mechanistic feature of aromatic growth, the zipper-growth mechanism.[34] This is a mechanism by which a zigzag edge can be sequentially built up after a nucleating ring has been formed either as a five-member ring in the interior of the edge or as a six-member ring at the corner. Briefly, the addition of a single five- or six-member ring to the zigzag surface creates one or more sites for subsequent six-member ring formation either through collision with a migrating five-member ring via reactions 14 or 27 or through direct gas-phase addition of acetylene via reactions 28, 33, or 34. In the following discussion, the term *corner nucleation* will be used to describe nucleation via six-member ring formation at the corner of the edge and *interior nucleation* for nucleation initiated by five-member ring adsorption in the middle of the edge. Depending on the length of the zigzag edge, a single nucleating site can catalyze growth of many more rings through repetition of reactions that fill in an armchair site.

The formation of embedded five-member rings creates a third avenue for zipper growth, via a reaction "capping" the embedded five-member ring. The sequence shown in Figure 3 illustrates such growth. In this mechanism, the "imperfect", armchair-like site created by the presence of the embedded ring can successively transform many zigzag sites into armchair sites. This type of zipper-growth nucleation will be referred to hereafter as *embedded-ring nucleation*. The location of the five-member ring when it is capped, as well as the length of the zigzag edge in which it is enclosed, determine the amount of armchair sites that are created. For example, in Figure 3 sixteen rings are able to add to the starting configuration, because the embedded five-member ring is located in the center. If the embedded ring were located three positions to the right instead, only seven rings would be able to add through armchair filling reactions. Note that the zipper-filling enabled by embedded five-member rings requires that the five-member ring be fully enclosed and therefore completely incorporated into the growing layer. This is different from lone five-member rings acting as nucleating sites which may then escape from the layer by migration.

The differences in growth rates and morphologies created by the relative contribution of corner, interior, and embedded-ring nucleation of zipper growth is a major feature of the present KMC simulations. Multiple interior nucleations on a single zigzag edge create unreactive regions. Lone and embedded-ring migration reactions have the potential to prevent defects from forming or removing them once formed.

Morphology. Representative graphene structures formed during growth of pyrene at 1500, 2000, and 2500 K are shown in Figure 4. Animations of the formation of these structures are included in the Supporting Information. Note, in the figure all of the edge carbon atoms are shown bonded to single hydrogen atoms. This is done for display purposes only; in the simulations the carbons may be of any type depicted in Figure 1. At 1500 K, five-member rings are more stable than at higher temperatures and therefore are more frequently incorporated into the growing structures. The increased stability of five-member rings at lower temperatures has two affects on the growth of the layer. The first affect is promotion of growth through the creation of interior zipper growth nucleation sites. The second affect hinders growth as incorporation of five-member rings creates portions of edge that are unable to grow. In the example

TABLE 1: KMC Reaction Steps

	reaction	rate coefficient	Ref
1	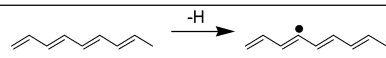	$k_1 = 4.2\times10^{13}e^{-8502/T}\ [\mathrm{H}]$	90
2	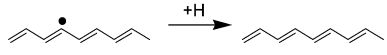	$k_2 = \frac{k_1}{7.59e^{-2097/T}}\frac{[\mathrm{H_2}]}{[\mathrm{H}]} + 2\times10^{13}[\mathrm{H}]$	52,91
3	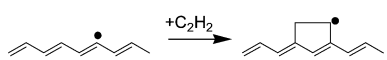	$k_3 = \frac{k_a k_b}{k_b + k_c + k_d}[\mathrm{C_2H_2}]$	34,51,*a*
4	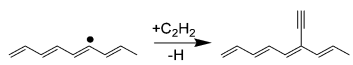	$k_4 = \frac{k_a k_d}{k_b + k_c + k_d}[\mathrm{C_2H_2}]$	34,*a*
5	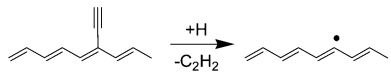	$k_5 = \frac{k_a k_e}{k_b + k_c + k_d}[\mathrm{H}]$	34,*a*
6	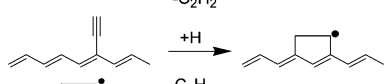	$k_6 = \frac{k_b k_e}{k_b + k_c + k_d}[\mathrm{H}]$	34,51,*a*
7	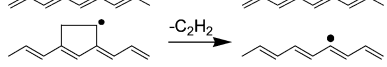	$k_7 = 3.1\times10^{11}T^{0.87}e^{-37403/T}$	52
8	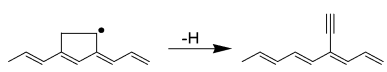	$k_8 = 6.7\times10^{11}T^{0.84}e^{-35625/T}$	52
9	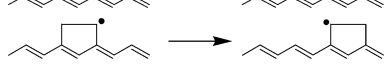	$k_9 = 1.3\times10^{11}T^{0.16}e^{-23099/T}$	52
10	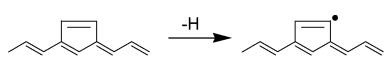	$k_{10} = 5.07\times10^{7}T^{1.93}e^{-6518/T}\ [\mathrm{H}]$	92
11	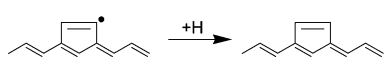	$k_{11} = 9.46\times10^{3}T^{2.56}e^{-2529/T}\ [\mathrm{H_2}] + 6.08\times10^{12}T^{0.27}e^{-141/T}\ [\mathrm{H}]$	92,93
12	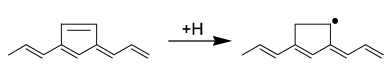	$k_{12} = 5.40\times10^{11}T^{0.45}e^{-916/T}\ [\mathrm{H}]$	93
13	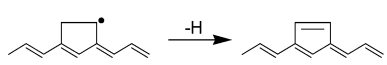	$k_{13} = \frac{k_{12}}{1.791e^{-17708/T}} + 2\times10^{12}[\mathrm{H}]$	93
14	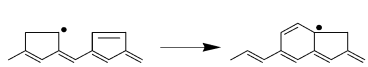	$k_{14} = 8.9\times10^{5}T^{2.28}e^{-30944/T}$	52
15	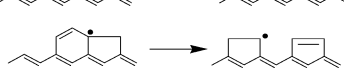	$k_{15} = 2.1\times10^{9}T^{1.14}e^{-41952/T}$	52
16	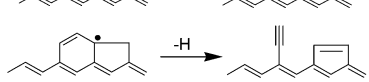	$k_{16} = 3.8\times10^{10}T^{1.30}e^{-51929/T}$	52
17	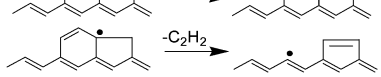	$k_{17} = 4.0\times10^{10}T^{1.53}e^{-57225/T}$	52
18	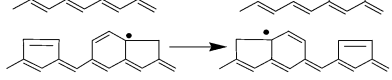	$k_{18} = k_{15}$	
19	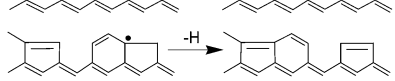	$k_{19} = k_{15}$	
20	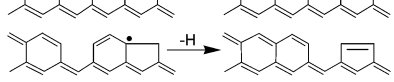	$k_{20} = k_{15}$	
21	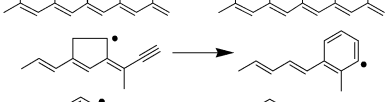	$k_{21} = k_9$	
22	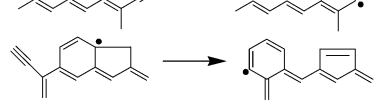	$k_{22} = k_{15}$	
23	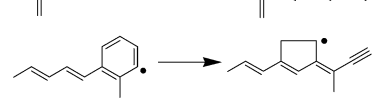	$k_{23} = \frac{k_9}{k_7 + k_8 + k_9}1.3\times10^{11}T^{1.08}e^{-35428/T}$	36
24	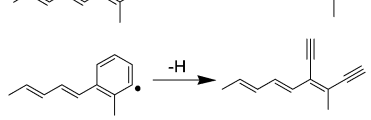	$k_{24} = \frac{k_8}{k_7 + k_8 + k_9}1.3\times10^{11}T^{1.08}e^{-35428/T}$	36
25	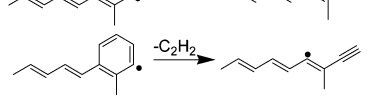	$k_{25} = \frac{k_7}{k_7 + k_8 + k_9}1.3\times10^{11}T^{1.08}e^{-35428/T}$	36
26	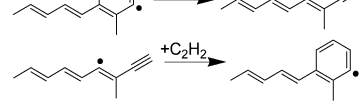	$k_{26} = \frac{k_a k_f}{k_c + k_d + k_f}[\mathrm{C_2H_2}]$	34
27	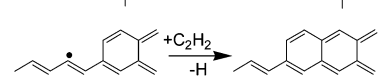	$k_{27} = 8.0\times10^{7}T^{1.56}e^{-1912/T}\ [\mathrm{C_2H_2}]$	36

TABLE 1: Continued

	reaction	rate coefficient	Ref
28	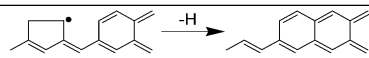	$k_{28} = k_9$	
29	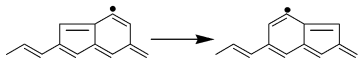	$p_{29} = 0.5$	53
30	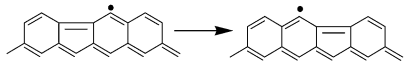	$p_{30} = 0.5$	54
31	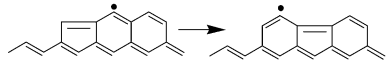	$p_{31} = 2/3$	54
32	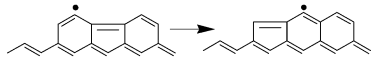	$p_{32} = 1/3$	54
33	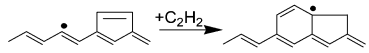	$k_{33} = \frac{k_{17}}{3.24\times10^3 e^{-52539/T}}[C_2H_2]$	52
34	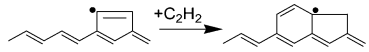	$k_{34} = k_{33}$	
35	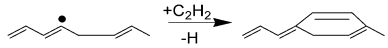	$k_{35} = k_3$	
36	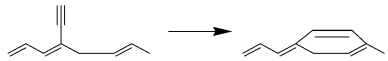	$k_{36} = k_6$	
37	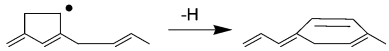	$k_{37} = k_9$	
38	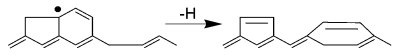	$k_{38} = k_{15}$	
39	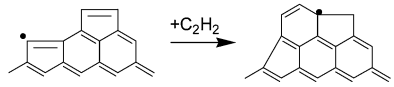	$k_{39} = k_{33}$	
40	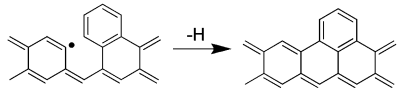	$k_{40} = 3.49\times10^{12} T^{-0.39} e^{-1228/T}$	39
41	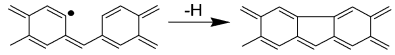	$k_{41} = 3.86\times10^{11} T^{-0.21} e^{-8908/T}$	58
42	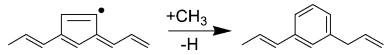	$k_{42} = 10^{13}[CH_3]$	*b*

[a] $k_a = 1.1 \times 10^7 T^{1.17} e^{-1960/T}$, $k_b = 6.8 \times 10^{11} e^{-11084/T}$, $k_c = 1.3 \times 10^{14} e^{-21025/T}$, $k_d = 4.8 \times 10^{12} e^{-16875/T}$, $k_e = 1.5 \times 10^{10} T^{0.85} e^{-601/T}$, $k_f = 2.5 \times 10^{12} T^{-0.13} e^{-7902/T}$. [b] Estimated (see Supporting Information).

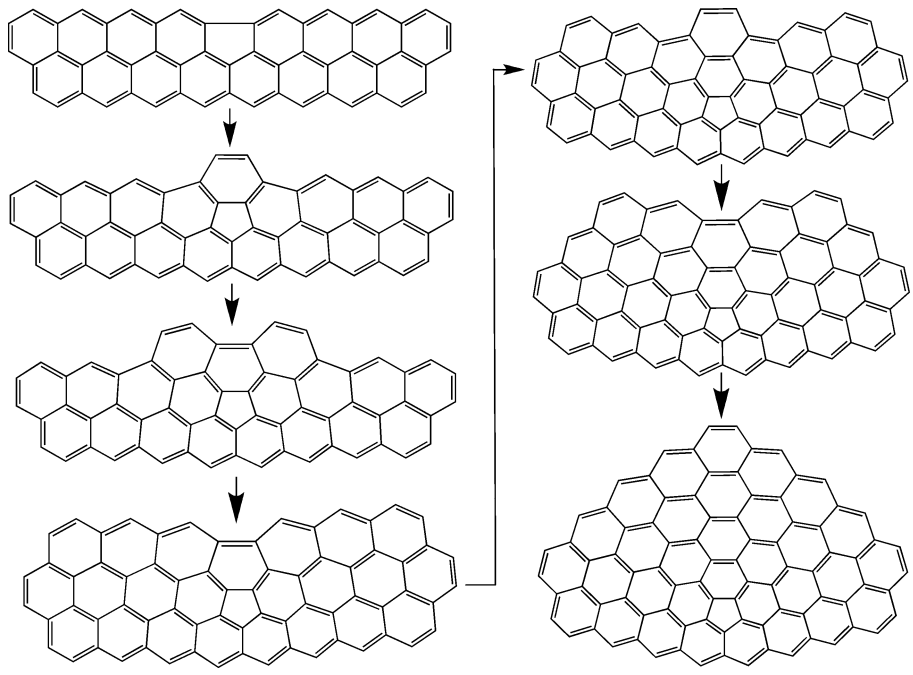

Figure 3. Embedded five-member ring facilitating zipper growth mechanism.

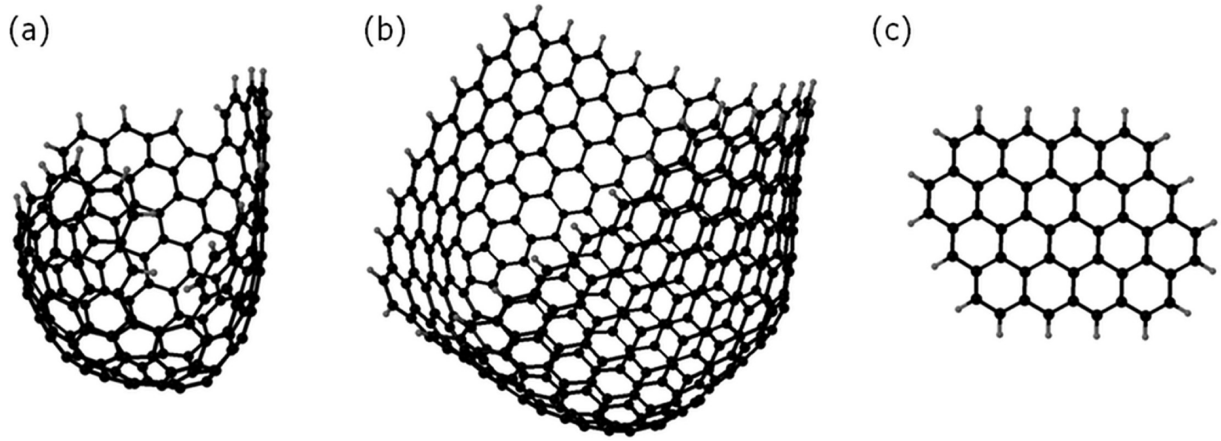

Figure 4. Representative structures resulting from pyrene growth at (a) 1500 K, (b) 2000 K, and (c) 2500 K.

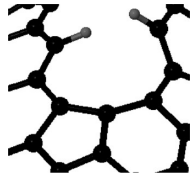

Figure 5. Detail of edge bifurcation in pyrene growth at 1500 K.

shown in Figure 4a, one can see bifurcation of the edge caused by the inclusion of five-member rings preventing formation of contiguous regions of zigzag edge, which in turn hinders zipper growth. A close up image of an edge bifurcation is shown in Figure 5.

The promoting and hindering affects of five-member rings described above are weighted in favor of growth at 2000 K. Five-member rings remain on the edge long enough to facilitate zipper growth. However, after catalyzing growth, the five-and-six-member ring complexes can fall apart through reactions like reaction 17, and subsequently the remaining five-member ring can desorb, leaving a structure composed of only six-member rings. After the layer has grown larger, the ability of embedded five-member rings to escape in this fashion decreases. The reason for the decreasing likelihood of desorption is that for reactions like reaction 17 to occur, the five- and six-member ring complex must not be enclosed by other rings. If an additional six-member ring exists on either side of the five- and six-member complex, there is essentially no way for the complex to fall apart. The result is that substrates growing at this temperature do not become curved until they are significantly larger than coronene. This phenomenon of transition from planar to curved growth can be seen in animation of growth at 2000 K included in the Supporting Information.

Growth of pyrene is much less frequent and five-member rings are rarely incorporated into the layer at 2500 K. The mechanism for growth at this temperature and substrate size is dominated by corner-nucleated zipper growth. Of the 15 simulations of pyrene growth that were run at 2500 K, seven grew to be larger than coronene. The structure shown in Figure 4c is one of those simulations. Of the other eight simulations, six did not grow at all, one ended as a structure composed of six aromatic rings, and one finished as coronene. None of the simulations of pyrene growth at 2500 K incorporated five-member rings into the structures due to the low stability of lone five-member rings at this temperature. On larger substrates, growth is more frequent at 2500 K. As the molecular structure gets larger, a single nucleation site enables more growth because a larger zigzag edge provides mores sites for rings to be added through the zipper filling mechanism.

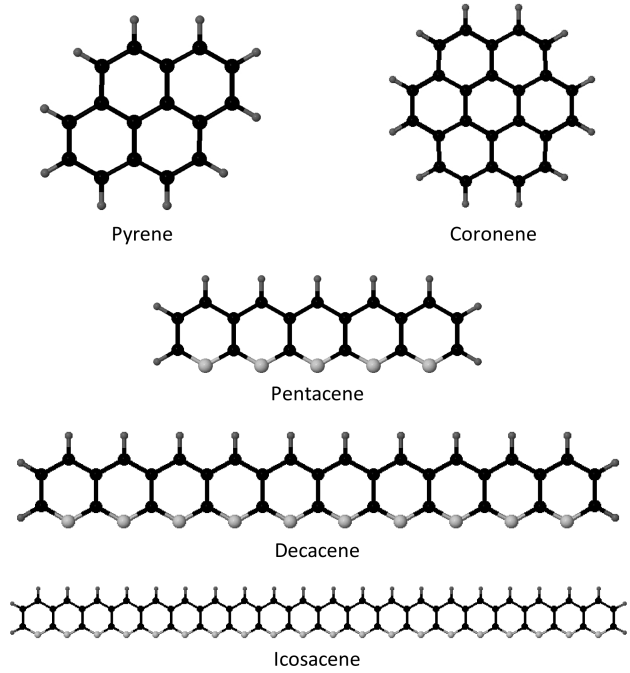

Figure 6. Starting substrates for surface kinetic Monte Carlo simulations. Hydrogen atoms are shown in dark gray, normal carbon in black, and solid carbon in light gray.

Effect of Initial Substrate. Five initial substrates were studied: pyrene, coronene, pentacene, decacene, and icosacene. The first two were allowed growth on all sites and thus were used to simulate the initial stages of soot precursor growth. The last three are linear acenes of five, ten, and twenty rings, respectively. The linear species were used as models for graphene layer (soot surface) growth and hence the lower row of carbon atoms was set as a1solid type to keep them from reacting. The five substrates are shown in Figure 6.

The rate of substrate growth was determined from a series of 15 simulation runs performed with different seeds for the random number generator for each substrate at each temperature. The calculations were typically carried out for 5 ms of simulated time. For some conditions, not all of the simulation runs were able to reach 5 ms before failing the consistency check between the optimized geometry and the bonding defined by the KMC simulation. In such cases, all the runs in the series were truncated so that the data presented are always the result of an average over a full series of 15 simulations.

The resulting data were used to calculate the average growth rate as a function of time for each series. Substrate growth was

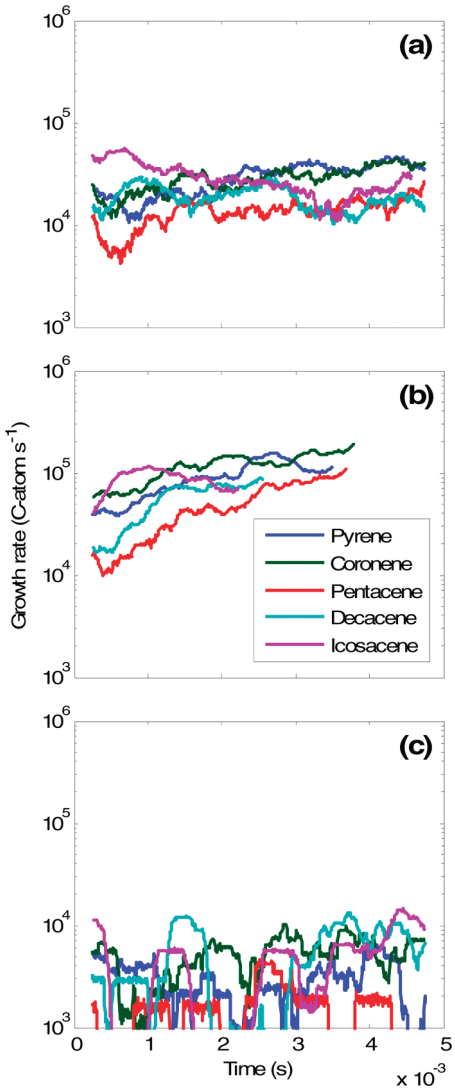

Figure 7. Substrate growth rates at (a) 1500 K, (b) 2000 K, and (c) 2500 K.

measured in the number of carbon atoms added to the initial substrate at each instant of time. Growth rates were then calculated by central-difference numerical differentiation of the average growth; i.e., the growth rate at time t_i was calculated as

$$\frac{G(t_{i+N}) - G(t_{i-N})}{t_{i+N} - t_{i-N}}$$

where G is the number of C-atoms. N was chosen to reduce noise due to stochastic fluctuations while maintaining high resolution of the data. Time intervals ($t_{i+N} - t_{i-N}$) were typically on the order of 0.5 ms. The resulting time dependent growth rates are plotted in Figure 7.

Inspection of the numerical results displayed in Figure 7 indicates that the growth rates for all substrates at 1500 K lie in the range of roughly (1−4) × 10^4 C-atoms s^{-1}, remaining fairly constant over the course of the simulations. At 2000 K, growth rates noticeably increase with time initially. At later times, all of the substrates tend toward growth rates of 10^5 C-atoms s^{-1}. At 2500 K, growth rates fluctuate much more but are generally in the range from 1 × 10^3 to 1 × 10^4 C-atoms s^{-1}. Growth at 2500 K is sporadic because corner nucleations are the dominant means of growth and are rare events given the low kinetic stability of C_2H adsorbate on the aromatic edge at this temperature.

To characterize the morphologies resulting from growth of different substrates at differing temperatures, we introduce a measure of incorporation of five-member rings, the *five-member-ring fraction*, defined as

$$f_{R5} = \frac{32}{12}\frac{N_{R5}}{N_{R5} + N_{R6}}$$

where N_{R5} and N_{R6} are the number of five-member and six-member rings, respectively, that comprise the molecular structure. The prefactor, 32/12, normalizes f_{R5} so that the buckminsterfullerene has an f_{R5} value of 1. The buckminsterfullerene is the smallest fullerene with no neighboring five-member rings and is composed of 12 five-member rings and 20 six-member rings. Given that five-member rings are not allowed to form next to each other in the kinetic mechanism and that a perfect graphene sheet has no five-member rings, f_{R5}, will range between zero (no five-member rings) and one (maximum number of five-member rings). Lone chemisorbed five-member rings are excluded from the calculation of f_{R5}.

The f_{R5} values obtained in the simulations with different substrates are plotted in Figure 8. Inspection of these results indicates that for all three temperatures, f_{R5} tends toward a constant value for each substrate. At 1500 K, the value is approximately 0.25 for all substrates. At 2000 K, the ending values of f_{R5} are much lower, around 0.05. Five-member ring incorporation is rare at 2500 K and so f_{R5} is zero for most of the substrates at this temperature. The nonzero values at later times for pentacene and decacene are the result of incorporation of a single five-member ring in a single simulation.

While higher values of f_{R5} translate to higher curvature, relatively small values can still lead to significant curvature. An example of such a structure is shown in Figure 9. It is produced in a simulation run of decacene growth at 2000 K and has an f_{R5} value of 0.1.

To further assess the morphology of growing structures, we also examined the number of edge bifurcations that an individual molecule develops. Edge bifurcations were discussed previously and are edge regions such as those shown in Figure 5. To identify their occurrences in numerical simulations, we defined an edge bifurcation as six or more solid carbon atoms in succession, of which at least one is classified as s2, i.e., that one of the carbon atoms is part of a five-member ring. Recovery from bifurcations is rare and therefore most bifurcations remain as part of the growing structure once they are formed.

The average number of edge bifurcations developed in simulations of the five substrates at 1500 and 2000 K is plotted in Figure 10. At 2500 K, growth is very smooth and no bifurcations were formed in any of our simulations at this temperature. The results at 1500 K demonstrate a significant effect of the initial substrate size on the number of edge bifurcations formed. Icosacene, the longest initial substrate, forms an average of 2.5 bifurcations in our simulations while pyrene, coronene, and pentacene form less than 1 on average. The longer edges of decacene and icosacene provide more opportunity for multiple nucleations (both corner and interior) to occur leaving gaps that cannot be filled in. At 2000 K, edge bifurcations are less common and the difference between the substrates is essentially gone.

Another measure we consider is the fraction of edge sites that can accommodate cyclization by addition of C_2H_2, f_{AC}. Such sites include armchair sites, zigzag sites, and armchair-like sites created by free and embedded five-member rings. The computed

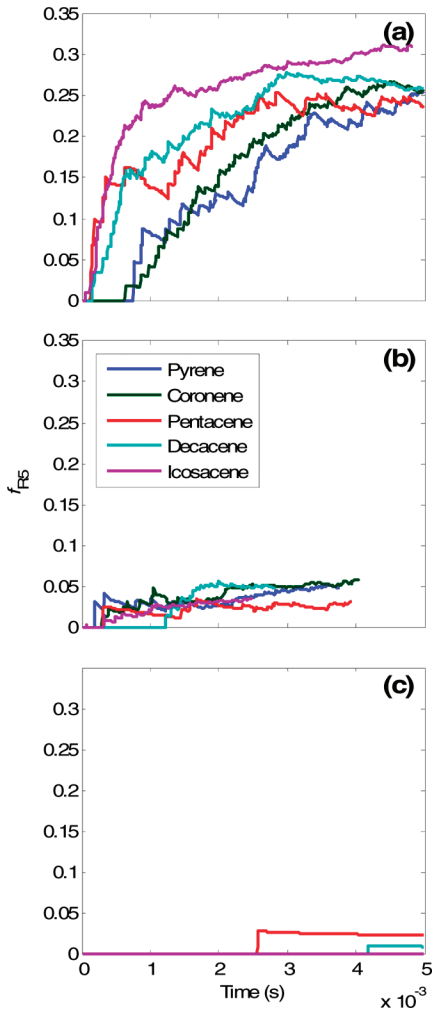

Figure 8. Five-member ring fraction at (a) 1500 K, (b) 2000 K, and (c) 2500 K.

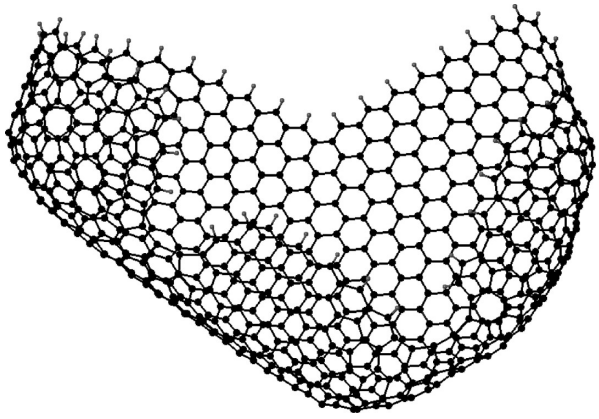

Figure 9. Example structure grown from decacene at 2000 K with $f_{R5} = 0.1$.

values of f_{AC}, plotted in Figure 11, tell a story similar to that for growth rate and f_{R5}. At 1500 K, f_{AC} values for different substrates converge quickly and decrease toward 0.4. At 2000 K, f_{AC} tends toward 0.8 for all substrates. At 2500 K, f_{AC} stays fairly constant for the linear substrates (pentacene, decacene, and isosacene) but increases with time for the molecular starting structures (pyrene and coronene). The nearly constant f_{AC} values for the linear substrates are due to stacking type growth caused by corner nucleation, in which each layer of added rings does not create many new growth sites. Starting with a molecular

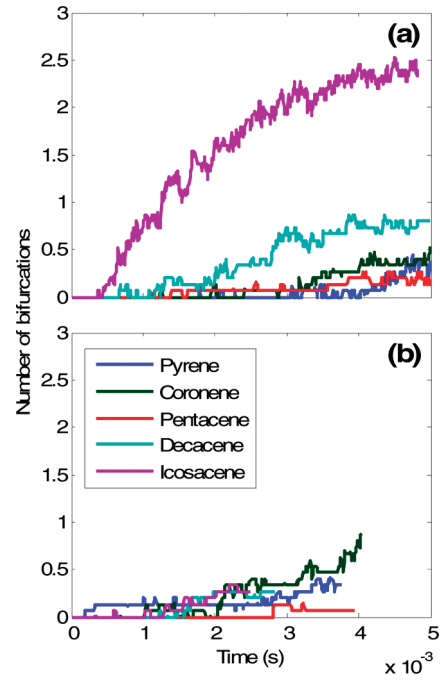

Figure 10. Average number of edge bifurcations at (a) 1500 and (b) 2000 K. At 2500 K (not shown) no bifurcations were formed.

substrate, a corner nucleation creates growth avenues along two edges and therefore creates more new growth sites per nucleation.

A few conclusions can be drawn from the comparison of growth of differing substrates as a function of temperature. First, growth rates lie mainly in the range of 10^3-10^5 C-atoms s^{-1}, with the slowest growth at 2500 K. This range and trend of growth rates are in agreement with the results of the FSP model[36] and hence comparable to initial rates of soot surface growth in laminar premised flames.[44,84,85] Convergence of growth rates, f_{R5}, and f_{AC} indicates that substrates become similar in nature as they grow, regardless of their initial configuration, at both 1500 and 2000 K. Finally, growing layers become significantly curved at the two lower temperatures, with the highest degree of curvature occurring at the lowest temperatures due to more frequent inclusion of five-member rings.

Effect of Reaction Exclusion. In the previous two sections, morphologies and growth were discussed for simulations that include all of the reactions listed in Table 1. In this section, we test the consequence of exclusion of key sets of reactions from the simulations. The tests are designed to gauge the effect of assumed rates for reactions in the kinetic mechanism. In light of the highly curved geometries that result from the full KMC model, we were particularly focused on curvature-inducing reactions.

Considering the stochastic nature of the model and the relatively large number of individual reaction steps, it is more informative and manageable to perform the tests by grouping reactions into related sets. The four reaction exclusion test cases were E1, reactions that create five- and six-member ring complexes (excludes reactions 14, 33, 34, 39, and 41); E2, reactions that cap embedded-five-member-rings (35, 36, 37, and 38); E3, flip and embedded-ring migration reactions (29, 30, 31, and 32); and E4, the combination of case E2 and case E3. Case E1 is similar to the FSP model,[36] and case E2 is similar to the Celnik et al. model.[37] Cases E3 and E4 are designed to test the importance of embedded-ring migration to structure evolution. Cases E1 through E4 were examined using coronene and decacene as substrates.

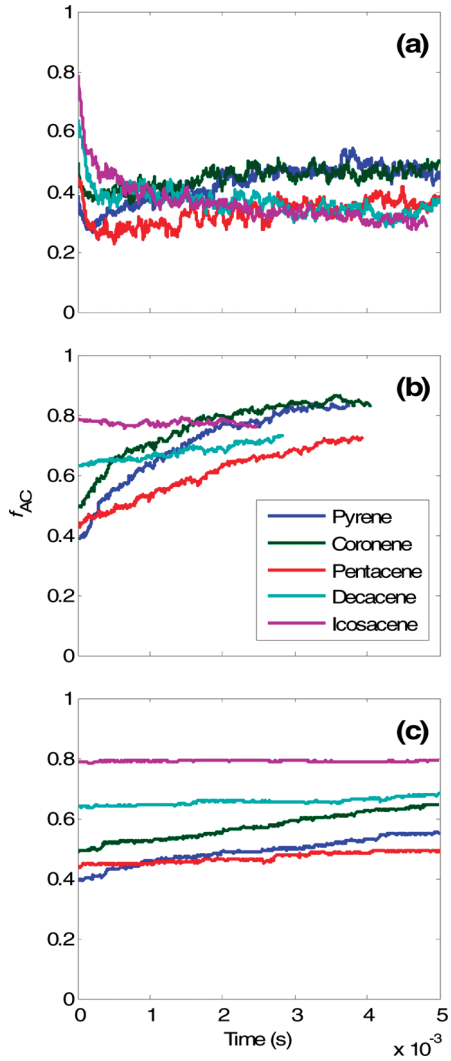

Figure 11. Fraction of edge sites accommodating cyclization at (a) 1500 K, (b) 2000 K, and (c) 2500 K.

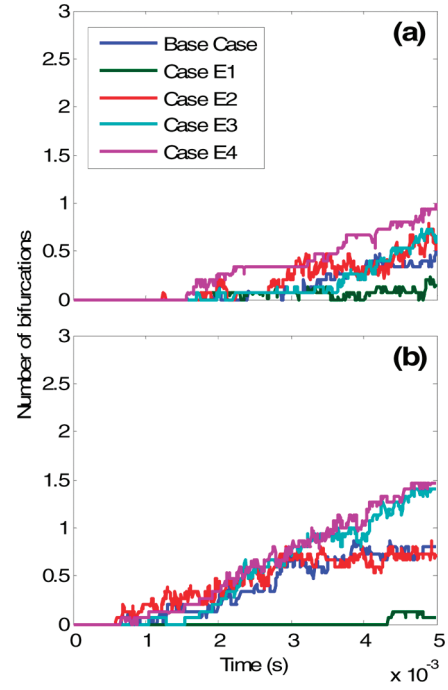

Figure 12. Average number of edge bifurcations for the reaction exclusion cases at 1500 K for (a) coronene and (b) decacene.

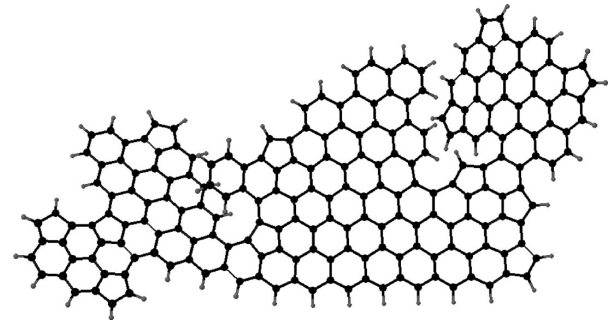

Figure 13. Morphology resulting from decacene growth at 1500 K, case E3, with $f_{R5} = 0.185$.

Growth rates are not significantly different between the five cases for either coronene or decacene at any of the three temperatures we studied. For almost all of the cases, the f_{R5} values are also not significantly affected. The exception is case E1 in which no five-member rings are incorporated and so the f_{R5} value for those cases is always zero, which results in completely planar, defect-free growth. However, in light of the present knowledge, this case is unlikely to be physically realistic. Of the reactions that form five- and six-member ring complexes (14, 33, 34, 39, and 41 in Table 1), two (34 and 39) have been assigned assumed rate coefficients, while the other three have rate coefficients calculated from quantum chemical results. Even if the rate coefficients of these reactions are overestimated and will have to be significantly reduced, five- and six-member ring complexes would still be formed and resulting five-member rings either will be capped and cause curvature or will exist as defects and thus create unreactive surface area.

Cases E2 through E4 show morphological differences that are not captured by the f_{R5} data but are to some extent captured in the number of bifurcations. Figure 12 shows the average number of edge bifurcations for the reaction exclusion cases compared with the base case at 1500 K for coronene and decacene. The biggest difference in the number of bifurcations is seen in case E1, in which edge bifurcations are almost absent. On the other hand, cases E3 and E4 increase the number of edge bifurcations for both coronene and decacene at 1500 K. Hence, disallowing embedded migration increases the roughness of the edge. This result is not surprising as surface migration of growth species is known to create smoother surfaces in a variety of growth processes.[86] The difference in the number of edge bifurcations is apparent in the resulting morphologies. An extreme example is shown in Figure 13 of a species growing from decacene at 1500 K in case E3.

The effect of reaction exclusion on the number of edge bifurcations at 2000 K is generally similar to that at 1500 K (see Figure 14). At 2000 K, edge bifurcations are most pronounced in case E4 followed by case E3. Edge bifurcations at 2000 K lead to the interesting phenomenon of stacked layers growing from a single substrate. Layer stacking happens following formation of an edge bifurcation, as the two resulting edges continue to grow next to each other. An example of the result of this behavior is shown in Figure 15. The separation between the two layers that results from the geometry optimization is ~3.5 Å, which is consistent with experimental measurements of layer separation in soot[41,87] and carbon black.[43,88]

At 2500 K, no edge bifurcation occurred in any of the studied cases. At this temperature growth is smooth in the base case and five-member rings are not involved in growth, and so the reaction exclusion cases do not make a significant difference to growth rates or morphology.

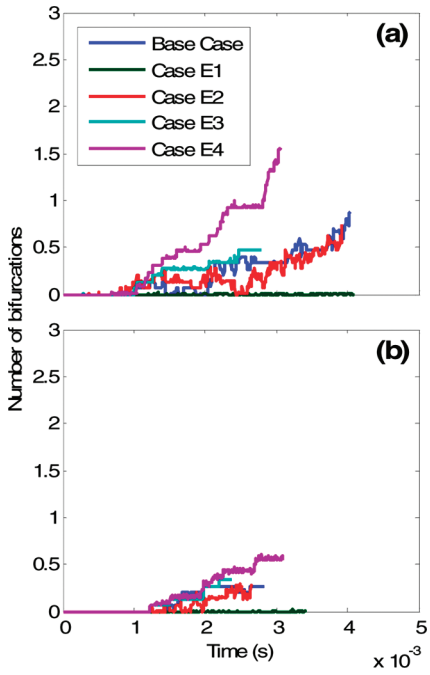

Figure 14. Average number of edge bifurcations for the reaction exclusion cases at 2000 K for (a) coronene and (b) decacene. The number of bifurcations for case E1 is nearly zero over the entire range for both substrates.

Effect of Gas-Phase Composition. We also examined the effect of altering the gas-phase composition on growth rates and morphology. The starting substrates for these calculations were coronene and decacene as they were in the reaction exclusion testing. Five gas-phase composition test cases were analyzed along with the base case, which was used in the preceding calculations. As discussed above, the base case composition is the same that was used in previous surface kinetic simulations[34,36] and is motivated by data from laminar flame studies.[48,83] The five test cases differ from the base case as follows: F1, C_2H_2 mole fraction reduced to 0.01; F2, H_2 mole fraction reduced to 0.01; F3, H mole fraction reduced to 0.001; F4, CH_3 mole fraction set to 0.01; and F5, CH_3 mole fraction set to 0.001. The last two cases "turn on" the reaction of methyl radical with edge five-member rings creating six-member rings (reaction 42 in Table 1) and vary its effective rate.

Growth rates of the two substrates at 1500 K comparing the various species concentrations are shown in Figure 16. Figures 17 and 18 compare f_{R5} and the number of edge bifurcations, respectively, for the concentration comparison cases. The most pronounced differences are seen in cases F1 and F4. Reduction of C_2H_2 in case F1 reduces the growth rate as one would expect. The slower growth leads to smoother surfaces embodied in the lower inclusion of five-member rings and a lower number of edge bifurcations. In contrast, case F4, with CH_3 mole fraction set to 0.01, leads to higher growth rates as the transformation of five-member rings to six-member rings through reaction 42 creates more nucleation sites, catalyzing growth. The faster growth leads to very rough surfaces with an average of over 2.5 edge bifurcations per simulation. The highly branched surfaces in turn lead to unphysical geometries that result in early termination of the simulations. The increased roughness occurs in spite of the fact that conversion of five-member rings to six-member rings reduces the number of five-member rings incorporated into the surface.

Cases F2, F3, and F5 have only a moderate effect at the simulation temperature of 1500 K. Of these, the most significant differences are seen in case F3, where reduction of the H-atom concentration leads to slightly reduced growth rate as a result of lower rate of surface activation via H abstraction (reaction 1). Case F3 also leads to a slight decrease in f_{R5}. The decrease in H-atom concentration relative to acetylene leads to an increase in corner nucleations, which at this temperature leads to a decrease in the number of five-member rings incorporated into the layer as fewer layers are added through interior nucleation.

Figures 19−21 show the growth rate, f_{R5}, and number of bifurcations, respectively, for the species concentration cases of coronene and decacene at 2000 K. At this temperature growth completely ceases for case F1. As a result, the f_{R5} and bifurcation plots are also zero for case F1. The only other case that deviates significantly from the base case at this temperature is case F3. The growth rate of this case is decreased from the base case due to formation of fewer edge radical sites because of lower H-atom concentration, as at 1500 K.

Note that the effect of the reduction in H concentration on the growth rate is more pronounced at 2000 K as compared to 1500 K. This can be explained by considering the kinetics of the following simplified reaction system

$$C_{edge}{-}H + H \underset{k_{-1}}{\overset{k_1}{\rightleftharpoons}} C_{edge}^{\bullet} + H_2$$

$$C_{edge}^{\bullet} + H \xrightarrow{k_2} C_{edge}{-}H$$

$$C_{edge}^{\bullet} \xrightarrow{k_3} \text{products}$$

where C_{edge} represents a "generic" edge carbon site (which could be that of a chemisorbed C_2H_2, for example). The rate of growth for this reaction sequence is proportional to the concentration of the radical, $C_{edge}^{\bullet}$, whose steady-state value is

$$[C_{edge}^{\bullet}] = \frac{k_1[C_{edge}{-}H][H]}{k_{-1}[H_2] + k_3 + k_2[H]}$$

The value of k_2 essentially does not depend on temperature, whereas those of k_{-1} and k_3 do. At low temperatures, when the k_2[H] term is larger than k_{-1}[H] and k_3, the [H] terms appearing in the numerator and denominator of the above ratio cancel out and the concentration of $C_{edge}^{\bullet}$ and hence the rate of growth do not depend on the concentration of H atoms. At high temperatures, when either the $k_{-1}[H_2]$ or k_3 term exceeds k_2[H], the $[C_{edge}^{\bullet}]$ and growth rate become proportional to [H].

More interestingly, f_{R5} increases for case F3 at 2000 K in contrast with its decrease at 1500 K. Corner nucleations are increased again at 2000 K due to decrease in H-atom concentration relative to C_2H_2. While at 1500 K this meant that fewer five-member rings were added through interior nucleation, at 2000 K growth is fast enough that corner nucleations can occur at both ends of an edge leading to a void in the middle of the edge that closes through reaction 41, creating a five-member ring. It is rings created in this fashion that increase the f_{R5} value for case F3 relative to the base case at this temperature.

At 2500 K, the only significant change in metrics for the five composition-comparison cases is in case F1 where growth is halted and so f_{R5} and the number of edge bifurcations are zero as a result. None of the other cases are significantly changed from the base case at this temperature.

IV. Summary

This study examined the evolution of growing graphene edges in combustion environments by combining a detailed description

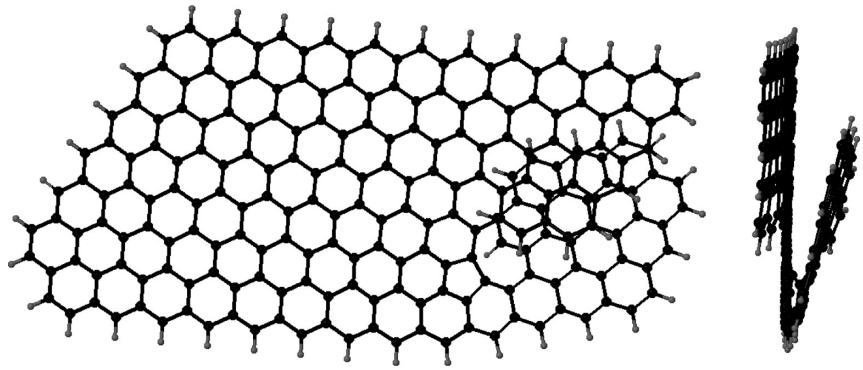

Figure 15. Front and side views of multiple layers growing from decacene substrate at 2000 K, case E4 with $f_{R5} = 0.031$.

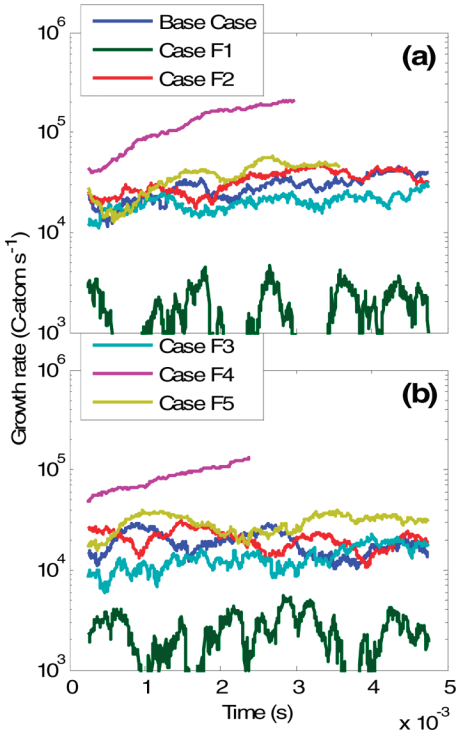

Figure 16. Growth rate comparing species fraction cases at 1500 K for (a) coronene and (b) decacene.

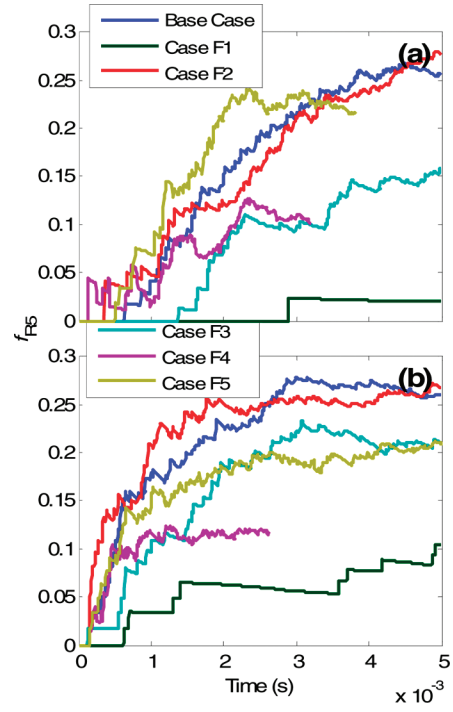

Figure 17. Five-member ring fraction comparing species fraction cases at 1500 K for (a) coronene and (b) decacene.

of surface chemistry with a relatively large number of reaction steps and molecular-mechanics optimization of resultant geometry. This allowed for the examination of the interplay of surface transformations and their effect on the formation of the different ring adsorption sites.

The simulation results demonstrate that evolving graphene morphology is significantly affected by varying temperature, gas-phase composition, and the rates of key reactions in the current kinetic model. Convergence with reaction time of numerical measures—growth rate, five-member-ring fraction f_{R5}, and fraction of edge sites that can accommodate cyclization by addition of acetylene f_{AC}—indicate that substrates become similar in nature as they grow, regardless of their initial configuration.

The computed growth rates lie mainly in the range from 10^3 to 10^5 C-atoms s^{-1}, in agreement with initial soot growth rates from the experiments of Harris and Weiner.[45,84,89]

Perhaps the most noteworthy feature of the present study is that growing layers become significantly curved. This occurs regardless of the initial substrate at both 1500 and 2000 K, although the lower temperature leads to the highest degree of curvature, caused by a higher rate of inclusion of five-member rings. More intriguing is the observation that transition from planar to curved growth at 2000 K does not commence immediately but occurs some later time, seemingly when the growing graphene reaches a size significantly larger than coronene. Identification and quantification of the factors controlling this transition could be a subject for future studies.

At 2500 K, the highest temperature used in our present simulations, we observed no graphene sheet curvature. In this high-energy environment, the five-member-ring intermediates become less thermodynamically and kinetically stable and do not form edge-embedded five-member rings. Perhaps this result could offer an explanation to the observation of very large, essentially "flat" graphene sheets in substrate-free microwave synthesis:[30,31] the generated plasma is sufficiently energetic to induce kinetic instability of five-member rings and thus prevent them from forming. Establishing the underlying mechanism of graphene growth in plasma-assisted synthesis could be another challenging area of future research.

It should also be noted that soot particles are composed of many layers of stacked aromatics. Such multilayer environments are likely to provide additional energetic and steric constraints and, as a consequence, will be less able to accommodate curvature than has been allowed in the present simulations. Proper consideration of multilayer graphene growth will require

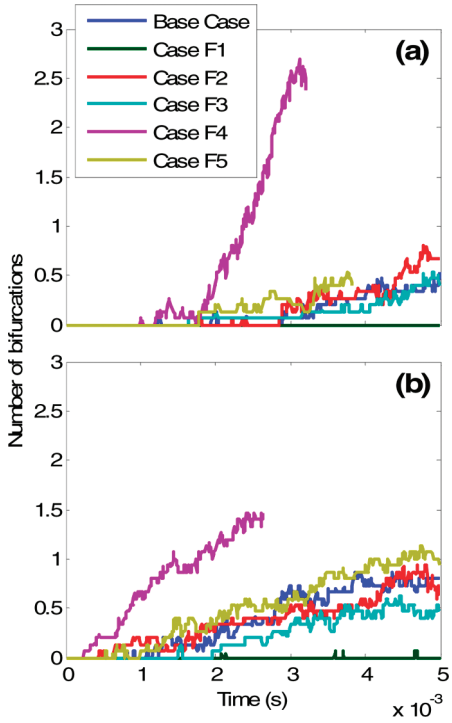

Figure 18. Average number of edge bifurcations for species fraction cases at 1500 K for (a) coronene and (b) decacene. The number of bifurcations for case E1 is nearly zero at all times at this temperature.

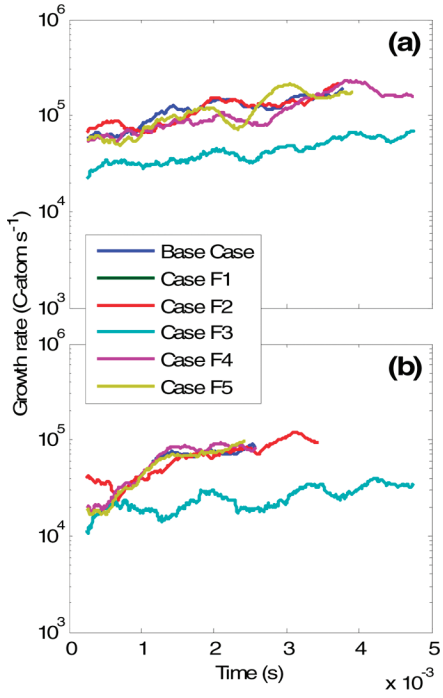

Figure 19. Growth rate comparing species fraction cases at 2000 K for (a) coronene and (b) decacene. The growth rate is zero at all times for case F1 on both substrates at this temperature.

extending the analysis to increasingly large molecular clusters, providing a nontrivial challenge to quantum chemistry.

It is likely that more elementary reactions will come to light as research in this area continues. The results of the present study already point to the needed work. The sensitivity of the morphologies to both embedded five-member ring migrations and to five-member ring capping reactions calls for a more thorough re-examination of such reactions. Another reaction that

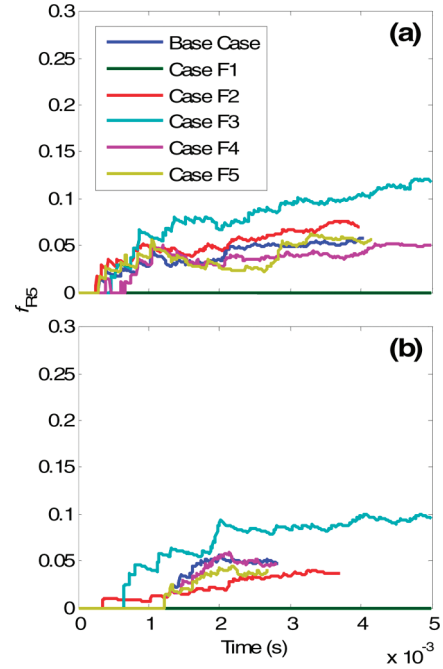

Figure 20. Five-member ring fraction comparing species fraction cases at 2000 K for (a) coronene and (b) decacene. Five-member ring fraction is zero for case F1 at all times at this temperature.

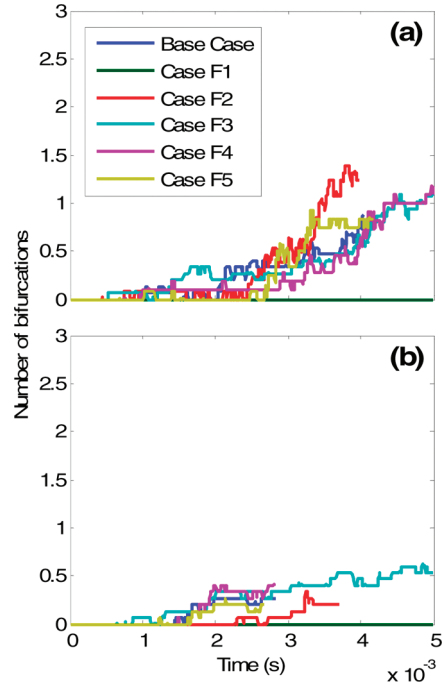

Figure 21. Average number of edge bifurcations for species fraction cases at 1500 K for (a) coronene and (b) decacene. No bifurcations were produced for case F1 on either substrate at this temperature.

needs attention is the transformation of a surface five-member ring into a six-member ring through combination with a methyl radical, which has a pronounced effect on the growth rate and morphologies at 1500 K. Finally, reactions that oxidize the graphene edge, while not included in the present study, should have a profound effect on graphene evolution in oxygen-containing environments.

Acknowledgment. This work was supported by the Director, Office of Energy Research, Office of Basic Energy Sciences,

Chemical Sciences, Geosciences and Biosciences Division of the U.S. Department of Energy, under Contract No. DE-AC03-76F00098.

Supporting Information Available: Details of reaction rate coefficients for KMC steps in Table 1 and animations of representative pyrene growth simulations. This material is available free of charge via the Internet at http://pubs.acs.org.

References and Notes

(1) Zhang, Y.; Tan, Y.-W.; Stormer, H. L.; Kim, P. *Nature* **2005**, *438*, 201–204.
(2) Novoselov, K. S.; Geim, A. K.; Morozov, S. V.; Jiang, D.; Katsnelson, M. I.; Grigorieva, I. V.; Dubonos, S. V.; Firsov, A. A. *Nature* **2005**, *438*, 197–200.
(3) Kane, C. L. *Nature* **2005**, *438*, 168–170.
(4) Balandin, A. A.; Ghosh, S.; Bao, W.; Calizo, I.; Teweldebrhan, D.; Miao, F.; Lau, C. N. *Nano Lett.* **2008**, *8*, 902–907.
(5) Lee, C.; Wei, X.; Kysar, J. W.; Hone, J. *Science* **2008**, *321*, 385–388.
(6) Geim, A. K.; Novoselov, K. S. *Nat. Mater.* **2007**, *6*, 183–191.
(7) Eda, G.; Chhowalla, M. *Nano Lett.* **2009**, *9*, 814–818.
(8) Zhang, Y.; Tang, T.-T.; Girit, C.; Hao, Z.; Martin, M. C.; Zettl, A.; Crommie, M. F.; Shen, Y. R.; Wang, F. *Nature* **2009**, *459*, 820–823.
(9) Chen, C.; Rosenblatt, S.; Bolotin, K. I.; Kalb, W.; Kim, P.; Kymissis, I.; Stormer, H. L.; Heinz, T. F.; Hone, J. *Nature Nanotech.* **2009**, *4*, 861−867.
(10) Xia, F. N.; Mueller, T.; Golizadeh-Mojarad, R.; Freitag, M.; Lin, Y. M.; Tsang, J.; Perebeinos, V.; Avouris, P. *Nano Lett.* **2009**, *9*, 1039–1044.
(11) Paek, S.-M.; Yoo, E.; Honma, I. *Nano Lett.* **2009**, *9*, 72–75.
(12) Wang, D. H.; Choi, D. W.; Li, J.; Yang, Z. G.; Nie, Z. M.; Kou, R.; Hu, D. H.; Wang, C. M.; Saraf, L. V.; Zhang, J. G.; Aksay, I. A.; Liu, J. *Acs Nano* **2009**, *3*, 907–914.
(13) Stoller, M. D.; Park, S. J.; Zhu, Y. W.; An, J. H.; Ruoff, R. S. *Nano Lett.* **2008**, *8*, 3498–3502.
(14) Lee, Z.; Jeon, K. J.; Dato, A.; Erni, R.; Richardson, T. J.; Frenklach, M.; Radmilovic, V. *Nano Lett.* **2009**, *9*, 3365–3369.
(15) Novoselov, K. S.; Geim, A. K.; Morozov, S. V.; Jiang, D.; Zhang, Y.; Dubonos, S. V.; Grigorieva, I. V.; Firsov, A. A. *Science* **2004**, *306*, 666–669.
(16) Meyer, J. C.; Geim, A. K.; Katsnelson, M. I.; Novoselov, K. S.; Booth, T. J.; Roth, S. *Nature* **2007**, *446*, 60–63.
(17) Stankovich, S.; Dikin, D. A.; Dommett, G. H. B.; Kohlhaas, K. M.; Zimney, E. J.; Stach, E. A.; Piner, R. D.; Nguyen, S. T.; Ruoff, R. S. *Nature* **2006**, *442*, 282–286.
(18) Park, S.; Ruoff, R. S. *Nat. Nanotechnol.* **2009**, *4*, 217–224.
(19) Kudin, K. N.; Ozbas, B.; Schniepp, H. C.; Prud'homme, R. K.; Aksay, I. A.; Car, R. *Nano Lett.* **2008**, *8*, 36–41.
(20) Berger, C.; Song, Z.; Li, X.; Wu, X.; Brown, N.; Naud, C.; Mayou, D.; Li, T.; Hass, J.; Marchenkov, A. N.; Conrad, E. H.; First, P. N.; de Heer, W. A. *Science* **2006**, *312*, 1191–1196.
(21) Chuang, A. T. H.; Boskovic, B. O.; Robertson, J. *Diamond Relat. Mater.* **2006**, *15*, 1103–1106.
(22) Chuang, A. T. H.; Robertson, J.; Boskovic, B. O.; Koziol, K. K. K. *Appl. Phys. Lett.* **2007**, *90*, 123107.
(23) Coraux, J.; N'Diaye, A. T.; Busse, C.; Michely, T. *Nano Lett.* **2008**, *8*, 565–570.
(24) Li, X. S.; Cai, W. W.; An, J. H.; Kim, S.; Nah, J.; Yang, D. X.; Piner, R.; Velamakanni, A.; Jung, I.; Tutuc, E.; Banerjee, S. K.; Colombo, L.; Ruoff, R. S. *Science* **2009**, *324*, 1312–1314.
(25) Kobayashi, K.; Tanimura, M.; Nakai, H.; Yoshimura, A.; Yoshimura, H.; Kojima, K.; Tachibana, M. *J. Appl. Phys.* **2007**, *101*, 094306.
(26) Marchini, S.; Gunther, S.; Wintterlin, J. *Phys. Rev. B* **2007**, *76*, 075429.
(27) Ueta, H.; Saida, M.; Nakai, C.; Yamada, Y.; Sasaki, M.; Yamamoto, S. *Surf. Sci.* **2004**, *560*, 183–190.
(28) Wang, J. J.; Zhu, M. Y.; Outlaw, R. A.; Zhao, X.; Manos, D. M.; Holloway, B. C. *Carbon* **2004**, *42*, 2867–2872.
(29) Zhao, X.; Outlaw, R. A.; Wang, J. J.; Zhu, M. Y.; Smith, G. D.; Holloway, B. C. *J. Chem. Phys.* **2006**, *124*, 094704.
(30) Dato, A.; Radmilovic, V.; Lee, Z.; Phillips, J.; Frenklach, M. *Nano Lett.* **2008**, *8*, 2012–2016.
(31) Dato, A.; Lee, Z.; Jeon, K. J.; Erni, R.; Radmilovic, V.; Richardson, T. J.; Frenklach, M. *Chem. Commun.* **2009**, *40*, 6095–6097.
(32) Subrahmanyam, K. S.; Panchakarla, L. S.; Govindaraj, A.; Rao, C. N. R. *J. Phys. Chem. C* **2009**, *113*, 4257–4259.
(33) Yuan, G. D.; Zhang, W. J.; Yang, Y.; Tang, Y. B.; Li, Y. Q.; Wang, J. X.; Meng, X. M.; He, Z. B.; Wu, C. M. L.; Bello, I.; Lee, C. S.; Lee, S. T. *Chem. Phys. Lett.* **2009**, *467*, 361–364.
(34) Frenklach, M. *Proc. Combust. Inst.* **1996**, *26*, 2285–2293.
(35) Frenklach, M.; Feigelson, E. In *From Stardust to Planetesimals*; Pendleton, Y. J., Tielens, A. G. G. M., Eds.; Astronomical Society of the Pacific: San Francisco, CA, 1997; pp 107−116.
(36) Frenklach, M.; Schuetz, C. A.; Ping, J. *Proc. Combust. Inst.* **2005**, *30*, 1389–1396.
(37) Celnik, M. S.; Raj, A.; West, R. H.; Patterson, R. I. A.; Kraft, M. *Combust. Flame* **2008**, *155*, 161–180.
(38) Celnik, M. S.; Sander, M.; Raj, A.; West, R. H.; Kraft, M. *Proc. Combust. Inst.* **2009**, *32*, 639–646.
(39) Raj, A.; Celnik, M.; Shirley, R.; Sander, M.; Patterson, R.; West, R.; Kraft, M. *Combust. Flame* **2009**, *156*, 896–913.
(40) Palmer, H. B.; Cullis, C. F. In *Chemistry and Physics of Carbon*; Walker, P. L., Ed.; Marcel Dekker: New York, 1965; Vol. 1, pp 265−325.
(41) Haynes, B. S.; Wagner, H. G. *Prog. Energy Combust. Sci.* **1981**, *7*, 229–273.
(42) Marchand, A. In *Polycyclic Aromatic Hydrocarbons and Astrophysics*; Léger, A., d'Hendecourt, L., Boccara, N., Eds.; Reidel: Dordrecht, Holland, 1987; pp 31−54.
(43) Kinoshita, K. *Carbon, Electrochemical and Physical Properties*; Wiley: New York, 1988.
(44) Harris, S. J.; Weiner, A. M. *Combust. Sci. Technol.* **1983**, *32*, 267–275.
(45) Harris, S. J.; Weiner, A. M. *Annu. Rev. Phys. Chem.* **1985**, *36*, 31–52.
(46) Sunderland, P. B.; Faeth, G. M. *Combust. Flame* **1996**, *105*, 132–146.
(47) Frenklach, M. In *Carbon in the Galaxy: Studies From Earth and Space*; Tarter, J. C., Chang, S., DeFrees, D. J., Eds.; NASA Conference Publication 3061; NASA: Washington, DC, 1990; pp 259−273.
(48) Frenklach, M.; Wang, H. *Proc. Combust. Inst.* **1991**, *23*, 1559–1566.
(49) Frenklach, M. *Phys. Chem. Chem. Phys.* **2002**, *4*, 2028–2037.
(50) Frenklach, M.; Clary, D. W.; Gardiner, W. C., Jr.; Stein, S. E. *Proc. Combust. Inst.* **1985**, *20*, 887–901.
(51) Frenklach, M.; Moriarty, N. W.; Brown, N. J. *Proc. Combust. Inst.* **1998**, *27*, 1655–1661.
(52) Whitesides, R.; Kollias, A. C.; Domin, D.; Lester, W. A., Jr.; Frenklach, M. *Proc. Combust. Inst.* **2007**, *31*, 539–546.
(53) Whitesides, R.; Domin, D.; Salomón-Ferrer, R.; Lester, W. A.; Frenklach, M. *J. Phys. Chem. A* **2008**, *112*, 2125–2130.
(54) Whitesides, R.; Domin, D.; Salomón-Ferrer, R.; Lester, W. A., Jr.; Frenklach, M. *Proc. Combust. Inst.* **2009**, *32*, 577–583.
(55) Kronholm, D. F.; Howard, J. B. *Proc. Combust. Inst.* **2000**, *28*, 2555–2561.
(56) Abid, A. D.; Heinz, N.; Tolmachoff, E. D.; Phares, D. J.; Campbell, C. S.; Wang, H. *Combust. Flame* **2008**, *154*, 775–788.
(57) Böhm, H.; Jander, H. *Phys. Chem. Chem. Phys.* **1999**, *1*, 3775–3781.
(58) Violi, A. *J. Phys. Chem. A* **2005**, *109*, 7781–7787.
(59) Park, J.; Burova, S.; Rodgers, A. S.; Lin, M. C. *J. Phys. Chem. A* **1999**, *103*, 9036–9041.
(60) Violi, A.; Kubota, A.; Truong, T. N.; Pitz, W. J.; Westbrook, C. K.; Sarofim, A. F. *Proc. Combust. Inst.* **2002**, *29*, 2343–2349.
(61) Violi, A.; Sarofim, A. F.; Voth, G. A. *Combust. Sci. Technol.* **2004**, *176*, 991–1005.
(62) Violi, A. *Combust. Flame* **2004**, *139*, 279–287.
(63) Violi, A.; Venkatnathan, A. *J. Chem. Phys.* **2006**, *125*, 054302.
(64) Chung, S. H.; Violi, A. *Carbon* **2007**, *45*, 2400–2410.
(65) Izvekov, S.; Violi, A. *J. Chem. Theory Comput.* **2006**, *2*, 504–512.
(66) Violi, A.; Izvekov, S. *Proc. Combust. Inst.* **2007**, *31*, 529–537.
(67) Fiedler, S. L.; Violi, A. *Carbon* **2007**, *45*, 1786–1794.
(68) Tidor, B. *J. Phys. Chem.* **1993**, *97*, 1069–1073.
(69) Pomeroy, J. M.; Jacobsen, J.; Hill, C. C.; Cooper, B. H.; Sethna, J. P. *Phys. Rev. B* **2002**, *66*, 235412.
(70) Zeifman, M. I.; Garrison, B. J.; Zhigilei, L. V. *J. Appl. Phys.* **2002**, *92*, 2181–2193.
(71) Grossmann, B.; Rancourt, D. G. *Phys. Rev. B* **1996**, *54*, 12294.
(72) Chiu, S. W.; Jakobsson, E.; Subramaniam, S.; Scott, H. L. *Biophys. J.* **1999**, *77*, 2462–2469.
(73) Chiu, S. W.; Jakobsson, E.; Scott, H. L. *Biophys. J.* **2001**, *80*, 1104–1114.
(74) Gillespie, D. T. *J. Phys. Chem.* **1977**, *81*, 2340–2361.
(75) Frenklach, M. *J. Chem. Phys.* **1992**, *97*, 5794–5802.
(76) Frenklach, M.; Clary, D. W.; Yuan, T.; Gardiner, W. C., Jr.; Stein, S. E. *Combust. Sci. Technol.* **1986**, *50*, 79–115.
(77) Frenklach, M.; Yuan, T.; Ramachandra, M. K. *Energy Fuels* **1988**, *2*, 462–480.
(78) Allinger, N. L.; Yuh, Y. H.; Lii, J.-H. *J. Am. Chem. Soc.* **1989**, *111*, 8551–8566.
(79) Ponder, J. W. *TINKER: Software Tools for Molecular Design*, version 4.2; Washington University School of Medicine: Saint Louis, MO, 2004; http://dasher.wustl.edu/tinker/.

(80) Murry, R. L.; Colt, J. R.; Scuseria, G. E. *J. Phys. Chem.* **1993**, *97*, 4954–4959.
(81) Schulman, J. M.; Disch, R. L. *J. Comput. Chem.* **1998**, *19*, 189–194.
(82) Whitesides, R. *Ph.D. Thesis*, University of California, Berkeley, 2009.
(83) Kazakov, A.; Wang, H.; Frenklach, M. *Combust. Flame* **1995**, *100*, 111–120.
(84) Harris, S. J.; Weiner, A. M. *Combust. Sci. Technol.* **1983**, *31*, 155–167.
(85) Xu, F.; Sunderland, P. B.; Faeth, G. M. *Combust. Flame* **1997**, *108*, 471–493.
(86) Barabási, A.-L.; Stanley, H. E. *Fractal Concepts in Surface growth*; Cambridge University: Cambridge, U.K., 1995.
(87) Ebert, L. B.; Scanlon, J. C.; Clausen, C. A. *Energy Fuels* **1988**, *2*, 438–445.
(88) Biscoe, J.; Warren, B. E. *J. Appl. Phys.* **1942**, *13*, 364–371.
(89) Harris, S. J.; Weiner, A. M. *Combust. Sci. Technol.* **1984**, *38*, 75–87.
(90) Kiefer, J. H.; Mizerka, L. J.; Patel, M. R.; Wei, H. C. *J. Phys. Chem.* **1985**, *89*, 2013–2019.
(91) Claire, P. d. S.; Barbarat, P.; Hase, W. L. *J. Chem. Phys.* **1994**, *101*, 2476–2488.
(92) Knyazev, V. D.; Bencsura, A.; Stoliarov, S. I.; Slagle, I. R. *J. Phys. Chem.* **1996**, *100*, 11346–11354.
(93) Smith, G. P.; Golden, D. M.; Frenklach, M.; Moriarty, N. W.; Eiteneer, B.; Goldenberg, M.; Bowman, C. T.; Hanson, R.; Song, S.; Gardiner, W. C.; Lissianski, V.; Qin, Z. http://www.me.berkeley.edu/gri_mech/, 1999.

JP906541A